NAVAL POSTGRADUATE SCHOOL
MONTEREY, CALIFORNIA

THESIS

FOUR QUADRANT DYNAMIC MODEL
OF THE
AUV II THRUSTER

by

James P. Brown

September, 1993

Thesis Advisor: Anthony J. Healey

REPORT DOCUMENTATION PAGE

Form Approved OMB No. 0704

1. AGENCY USE ONLY *(Leave blank)*	2. REPORT DATE	3. REPORT TYPE AND DATES COVERED
	September, 1993.	Master's Thesis

4. TITLE AND SUBTITLE FOUR QUADRANT DYNAMIC MODEL OF THE AUV II THRUSTER

5. FUNDING NUMBERS

6. AUTHOR(S) Brown, James P.

7. PERFORMING ORGANIZATION NAME(S) AND ADDRESS(ES)
Naval Postgraduate School
Monterey CA 93943-5000

8. PERFORMING ORGANIZATION REPORT NUMBER

9. SPONSORING/MONITORING AGENCY NAME(S) AND ADDRESS(ES)

10. SPONSORING/MONITORING AGENCY REPORT NUMBER

11. SUPPLEMENTARY NOTES The views expressed in this thesis are those of the author and do not reflect the official policy or position of the Department of Defense or the U.S. Government.

12a. DISTRIBUTION/AVAILABILITY STATEMENT
Approved for public release; distribution is unlimited.

12b. DISTRIBUTION CODE
*A

13. ABSTRACT *(maximum 200 words)*

The dynamic behavior of the AUV II thruster was mathematically modeled by a four quadrant mapping of the propeller blade lift/drag coefficients as a function of f..id effective angle of attack. The model was validated with experimental transient response test tank data of the actual AUV II thruster, yielding improved predicted results with respect to previous thruster models. An open loop static mapping control law was formulated, simulated, and evaluated utilizing the new model.

14. SUBJECT TERMS THRUSTER, DYNAMIC RESPONSE, AUTONOMOUS UNDERWATER VEHICLES(AUV)

15. NUMBER OF PAGES *52

16. PRICE CODE

17. SECURITY CLASSIFICATION OF REPORT	18. SECURITY CLASSIFICATION OF THIS PAGE	19. SECURITY CLASSIFICATION OF ABSTRACT	20. LIMITATION OF ABSTRACT
Unclassified	Unclassified	Unclassified	UL

NSN 7540-01-280-5500

Standard Form 298 (Rev. 2-89)
Prescribed by ANSI Std. 239-18

Approved for public release; distribution is unlimited.

FOUR QUADRANT DYNAMIC MODEL
of the
AUV II THRUSTER

by

James P. Brown
Lieutenant Commander, United States Navy
B.A., Western Maryland College

Submitted in partial fulfillment
of the requirements for the degree of

MASTER OF SCIENCE IN MECHANICAL ENGINEERING

from the

NAVAL POSTGRADUATE SCHOOL
September, 1993

Author: 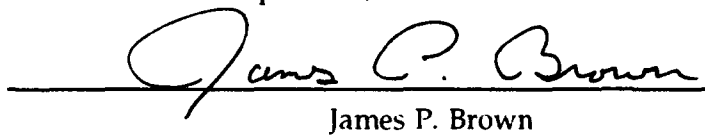

James P. Brown

Approved by: 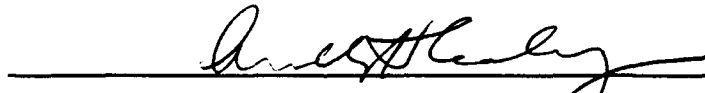

Anthony J. Healey, Thesis Advisor

Matthew D. Kelleher, Chairman
Department of Mechanical Engineering

ABSTRACT

The dynamic behavior of the AUV II thruster was mathematically modeled by a four quadrant mapping of the propeller blade lift/drag coefficients as a function of fluid effective angle of attack. The model was validated with experimental transient response test tank data of the actual AUV II thruster, yielding improved predicted results with respect to previous models. Open loop inverse static mapping control was formulated and simulated utilizing the new model.

TABLE OF CONTENTS

LIST OF FIGURES

NOMENCLATURE

D	Diameter of the tunnel
A	Cross sectional area of the tunnel and propeller
L	Length of the tunnel
J_M	Motor Polar Moment of Inertia
J_{DG}	Pinion Polar Moment of Inertia
J_P	Propeller Polar Moment of Inertia
C_M	Motor Shaft Friction
C_P	Propeller Shaft Friction
R	Motor Electrical Resistance
K_M	Motor Back EMF Constant
K_T	Motor Torque Constant
V_s	Motor voltage
i_a	Motor current
U_p	Propeller linear velocity
U_a	Water column linear velocity
v	Total relative velocity
ω_m	Motor angular velocity
F_a	Axial thrust
τ_{hydro}	Hydrodynamic torque
N	Reduction Gear Ratio
ρ	Water density

ACKNOWLEDGMENTS

I would like to thank Dr. Anthony Healey for his support and guidance during my work on this thesis. Also Mike Lee of MBARI for his technical collaboration and the NPS Direct Research Fund for the financial backing needed for this work.

I. INTRODUCTION

A. BACKGROUND

Autonomous Underwater Vehicles (AUV) and Remotely Operated Vehicles (ROV) are performing increasingly complex tasks and missions, including search, survey, sensor placement, and sensory data gathering. The slow speed positioning and hovering of the vehicles during these tasks is accomplished by vertical and horizontal thrusters. Accurate positioning of the vehicles requires a thorough understanding of the thrusters, the forces they produce, and ultimately the effects on the vehicle.

Researchers at Woods Hole Oceanographic Institute noted that closed loop control of shrouded thrusters commonly found on ROV's may produce limit cycles and positioning hysteresis problems even if the system experienced no external disturbances [Ref. 3]. Naval Postgraduate School researchers modeled the tunneled thruster on the AUV II pictured in Figure 1.1. By incorporating the acceleration of the tunnel's added mass, the NPS model predicted that system stability may be enhanced by the influence of the tunnel [Ref. 1 and 2]. Evaluation of both models by Miles of the Monterey Bay Aquarium Research Institute [Ref. 4] indicated that neither model accurately described the rapid acceleration of small thruster propeller blades and the effects of fluid angle of attack on the blades.

While there is a long history of work on propeller modeling, the usual focus is on propeller efficiency at constant forward speed for large ships and submarines. The much

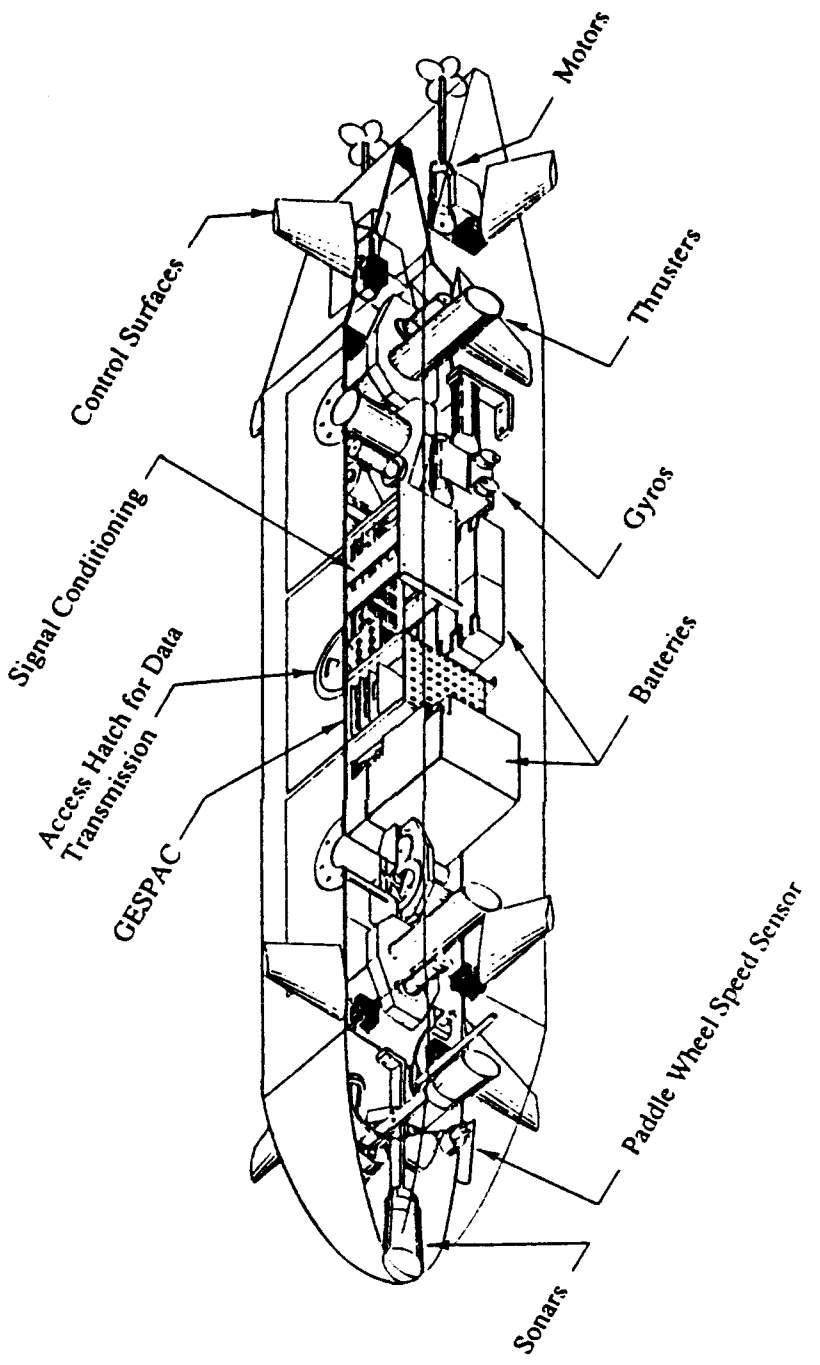

Figure 1.1 Naval Postgraduate School AUV II

smaller size of AUV's and ROV's, and the corresponding fast response of the vehicles and their thrusters during dynamic positioning requires an understanding of the full dynamic range of the thruster to insure motion stability.

An improved thruster dynamic model must include a full four quadrant representation of propeller thrust and torque for both directions of propeller and fluid velocity to cover the full range of thruster operation. A similar approach was previously done at the Netherlands Ship Model Basin [Ref. 6] which used extensive experimental data to develop a four quadrant model of thrust and torque coefficients as a function of effective angle of attack for a series of B-screws. The coefficient curves where reduced to 10 or 20 term Fourier series expansions for use in models for propeller design and simulation of emergency backing bell maneuvers. It was found that the coefficient curves developed for these B-screws do not necessarily transfer for modeling of different propellers.

In a study of cycloidal propellers [Ref. 7] lift/drag coefficient curves including blade stall as a function of effective angle of attack for cycloidal blades were proposed. Several unknown parameters had to be identified to match the curves to a particular propeller. This method was not directly applicable to thruster propellers but was adapted and used as the basis for the AUV II thruster model.

B. SCOPE OF THESIS

The scope of this thesis is to expand upon Miles' analysis of dynamic first quadrant thruster operation, and to propose a simple lift/drag mapping over four quadrant

operation while requiring only two disposable parameters to define the mapping, the maximum lift and drag coefficients. If the assumed functional form can be verified as appropriate, this improved model could be applicable to other thruster models where only a few parameters would need to be identified from simple experiments.

Using the hypothesized lift/drag mapping, this work will compare the predicted results of the improved NPS model with experimental data recorded by Cody [Ref. 1], and derive a suitable control law for the AUV II thruster. Use of the control law in the vehicle during in water missions is the final result of this thesis.

Chapter II will show the derivations of the two first order nonlinear coupled differential equations that model the thruster. Chapter III will validate the theoretical model with experimental data. Chapter IV will propose a control scheme and simulate thruster response. Chapter V will present the conclusions and recommendations of this thesis.

II. THEORETICAL THRUSTER MODEL

A. THRUSTER DESCRIPTION

The AUV II has two sets of thrusters forward and aft, mounted internal to the vehicle as shown in Figure 1.1. Each set has one vertical and one horizontal thruster assembly which allows for slow speed maneuvering, hovering, and station keeping. The internal mounting reduces drag on the vehicle during normal flight. Each of the four thrusters are a complete unit and identical except the horizontal tunnel is 16.5 inches long and the vertical tunnel is 10 inches. For the remainder of this thesis only the horizontal thruster will be considered.

Figure 2.1 shows a cross section view of the thruster assembly. The four basic subassemblies are a DC servomotor, a set of reduction gears, a propeller, and the thruster tunnel. The small diameter of the tunnel requires the servomotor to drive the propeller with a gear train vice mounting the propeller on the motor shaft. This is the same configuration use for earlier experimental and theoretical work on the NPS AUV II thruster.

1. Servomotor

The following is a description of the DC servomotor.

- Type- Pittman PITMO DC MODEL 14202
- Size- 2.125 in. diameter by 3.4 in. length
- Speed- 3820 RPM (no load)

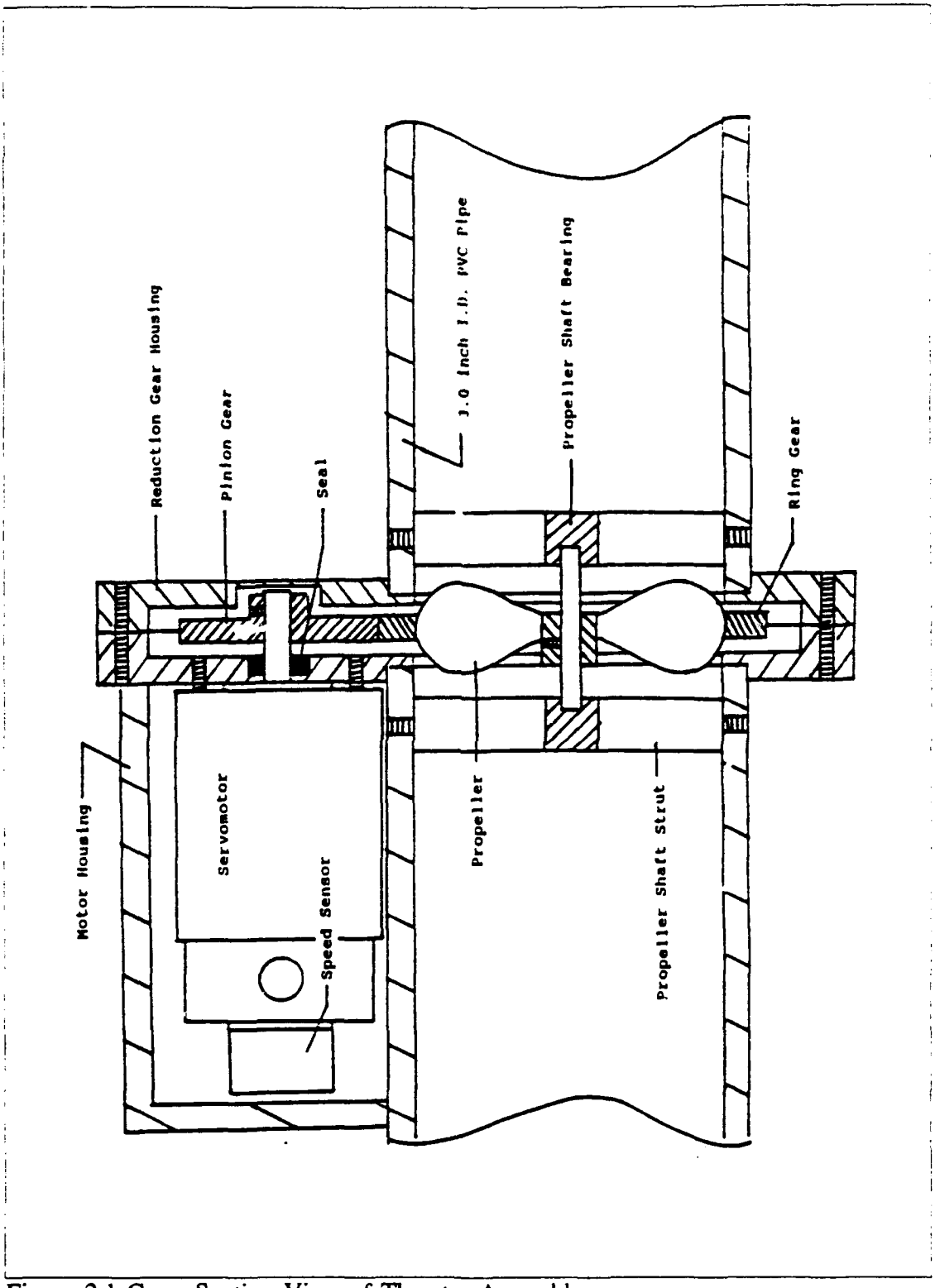

Figure 2.1 Cross Section View of Thruster Assembly

- Torque- 106 ounce-inches (stall)
- Volt- 24 volts
- Current- 0.230 amps (no load)
- Power- 333 watts (peak)

Motor speed is controlled by a PWM Servo Amplifier Model 30A8DD which uses a zero to ten volt control signal to modulate the pulse width of a load dependent 24 volt, 5 - 45 KHz output signal to the motor. Motor direction is controlled by changing the polarity of the control signal.

2. Reduction Gears

The propeller is driven by the servomotor through a set of spur gears with a 2:1 reduction ratio. The gear set has the following specifications.

- Pinion- 45 teeth, 24 pitch, 1.875 in. pitch diameter
- Gear- 90 teeth, 24 pitch, 3.75 in. pitch diameter

The gear is a ring gear with the propeller rigidly affixed to the inside of the ring.

3. Propeller

The propeller was fabricated locally in the NPS machine shop. The 3.0 inch diameter matches the I.D. of the tunnel. The four blades are Kaplan type with 45 degree pitch and zero camber allowing for equally effective forward and reverse operation. Propeller thrust is transferred through two thrust/journal bearings and axially mounted struts.

4. Thruster Tunnel

Each tunnel is constructed of 3.0 inch I.D., schedule 40 PVC pipe. The 16.5 inch horizontal and 10.0 inch vertical tunnels match the inside dimensions of the AUV II body. The servomotor, gear, propeller subassemblies are located at the midpoint of each tunnel.

B. DYNAMIC MODELING

The foundation for this development is based on two previously published dynamic thruster models. Cody [Ref. 1] and McLean [Ref. 2] developed the NPS model based on the NPS AUV II tunnel thruster. Yoerger, Cooke, and Slotine [Ref. 3] based their model on shrouded thrusters. Both used lumped mass, one dimensional techniques. The major difference between the models is that McLean/Cody included the acceleration of a cylinder of water through the thruster tunnel. The inclusion of the water column acceleration term causes the NPS model to predict a lead response to step inputs while the WHOI model predicts a lag response.

Research by Miles [Ref. 4] and Adams [Ref. 5] suggested that better predicted response from the two models is possible if the changes in the effective angle of attack of the water column on the propeller during rapid propeller speed changes is considered. The velocity of the water column will lag the velocity of the propeller, causing the effective angle of attack on the blades to change, resulting in varying thrust output. The previous models related the volumetric flow rate of the water column and the thrust produced by the propeller only to the propeller velocity.

This thesis will propose a simple four quadrant lift/drag model where propeller performance is variable throughout the entire range of propeller/water column velocities and changes as a function of the fluid effective angles of attack on the propeller blades. This is done while requiring only two uncertain parameters, the maximum lift and drag coefficients, to completely characterize the propeller performance. The overall thruster model is divided into three parts; electrical, mechanical, and hydrodynamic. The equations developed in these three areas will be combined into a set of two non-linear differential equations which are a function of two state variables, motor angular velocity ω_m and water column linear velocity U_a. The proposed four quadrant mapping provides the linkage between the state variables, the thruster axial force, and the propeller's hydrodynamic load torque.

1. Electrical Model

This is a standard dynamical model of a DC servomotor found in introductory controls textbooks. Figure 2.2 is a schematic of both the electric and mechanical systems.

The motor law states that the torque produced by the motor is proportional to the armature current.

$$\tau_{elect} = K_T i_a$$

The generator law states that back-EMF is proportional to the motor angular velocity.

$$e = K_M \omega_M$$

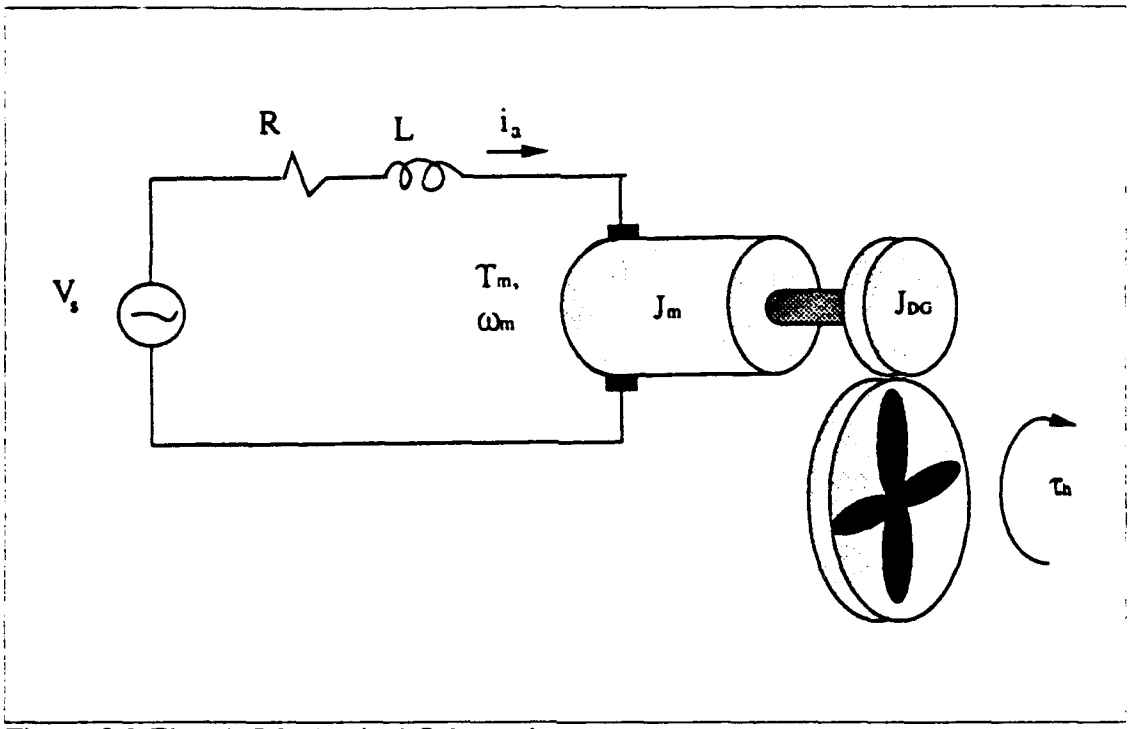

Figure 2.2 Electric/Mechanical Schematic

Assuming winding inductance is negligible, solve Kirchoff's voltage law for current.

$$i_a = \frac{V_s - e}{R}$$

Substituting for current and back-EMF into the motor torque equation gives servomotor torque as a function of applied voltage and the motor angular velocity.

$$\tau_{elect} = \frac{K_T}{R} V_s - \frac{K_T K_M}{R} \omega_M \qquad (2.1)$$

2. Mechanical Model

The mechanical torque as seen by the servomotor is a sum of the inertial, frictional, and hydrodynamic loads on the motor shaft, drive gear, and propeller.

$$\tau_{mech} = \tau_{motor} + \tau_{gear} + \frac{\tau_{prop} + \tau_{hydro}}{N}$$

The motor shaft and drive gear torque is related to motor velocity and acceleration.

$$\tau_{motor} + \tau_{gear} = (J_M + J_{DG})\dot{\omega}_M + C_M\omega_M$$

The propeller torque is related to the propeller velocity and acceleration.

$$\tau_{prop} = J_P\dot{\omega}_P + C_P\omega_P$$

Noting that motor and propeller velocity are related by the reduction ratio,

$$\omega_M = N\omega_P$$

the above equations can be combined in terms of motor velocity and acceleration.

$$\tau_{mech} = \left(J_M + J_{DG} + \frac{J_P}{N^2}\right)\dot{\omega}_M + \left(C_M + \frac{C_P}{N^2}\right)\omega_M + \frac{\tau_{hydro}}{N} \qquad (2.2)$$

Equating the torque produced by the servomotor and the load torque of the mechanical system,

$$\tau_{mech} = \tau_{elect}$$

$$\left(J_M + J_{DG} + \frac{J_P}{N^2}\right)\dot{\omega}_M = -\left(C_M + \frac{C_P}{N^2} + \frac{K_T K_M}{R}\right)\omega_M + \left(\frac{K_T}{R}\right)V_a - \frac{\tau_{hydro}}{N} \qquad (2.3)$$

Simplify by letting,

$$K_0 = \left(C_M + \frac{C_P}{N^2} + \frac{K_T K_M}{R}\right)$$

and

$$K_1 = \left(\frac{K_T}{R}\right)$$

and

$$K_2 = \left(J_M + J_{DG} + \frac{J_P}{N^2}\right)$$

Substitution results in the following first order differential equation:

$$\dot{\omega}_M = -\left(\frac{K_0}{K_2}\right)\omega_M + \left(\frac{K_1}{K_2}\right)V_a - \frac{\tau_{hydro}}{K_2 N} \tag{2.4}$$

This is the first system dynamic equation where motor velocity is the state variable and motor voltage is the system input.

$$\dot{\omega}_M = f_1(\omega_M, \tau_{hydro}, V_a)$$

3. Hydrodynamic Model

McLean [Ref. 2] derived a control volume, conservation of momentum equation for the thrust produced by a tunnel thruster which will be presented here without derivation.

$$F_a = (\rho AL\gamma)\dot{U}_a + (\rho A\Delta\beta)U_a|U_a| \tag{2.5}$$

Let

$$K_3 = (\rho AL\gamma)$$

and

$$K_4 = (\rho A\Delta\beta)$$

Substitute and solve for water column acceleration.

$$\dot{U}_a = \frac{(F_a - K_4 U_a |U_a|)}{K_3} \tag{2.6}$$

Equation 2.6 is the second system dynamic equation where water column velocity is the state variable. In summary the two system differential equations are,

$$\begin{aligned} \dot{\omega}_M &= f_1(\omega_M, \tau_{hydro}, V_a) \\ \dot{U}_a &= f_2(U_a, F_a) \end{aligned} \tag{2.7}$$

Figure 2.3 is the block diagram of the desired overall system model. The blocks for the tunnel and motor model have been derived in equations 2.7. The blocks that transform the state variables to axial force and hydrodynamic force will be derived next.

4. Combined Four Quadrant Model

Realizing that motor angular velocity is related to propeller linear wheel velocity U_p by,

$$U_p = 0.7\left(\frac{D}{2}\right)\frac{\omega_M}{N}$$

U_p and U_a determine the magnitude of the total relative velocity of fluid over the blade;

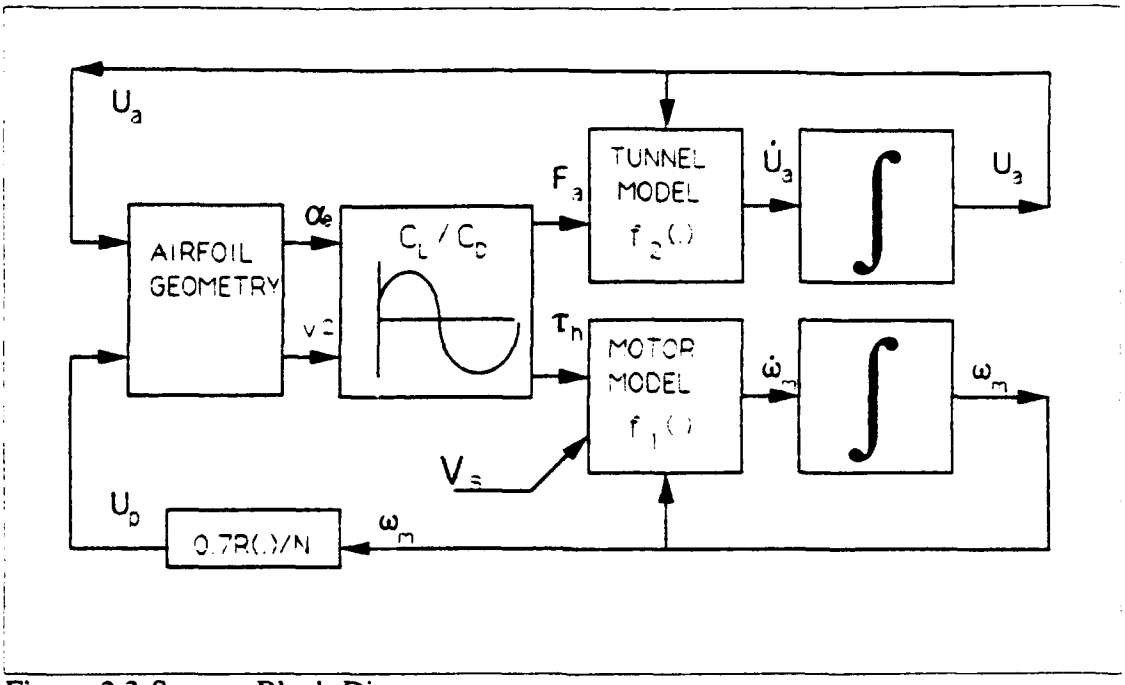

Figure 2.3 System Block Diagram

$$v^2 = U_a^2 + U_p^2$$

Figure 2.4 shows the relationship of the magnitude and direction of total velocity as a function of the state variables as they change direction. Quadrants I and III are the steady state regions where U_a and U_p are both in the same direction. Quadrants II and IV are transient conditions where the propeller has changed direction and water column velocity is lagging propeller velocity.

Figure 2.5 shows the geometric relationship between the state variables, the relative flow angle, and the effective angle of attack.

$$\theta = \arctan\left(\frac{U_a}{U_p}\right)$$

$$\alpha_e = \left(\frac{\pi}{2} - \text{pitch}\right) - \theta$$

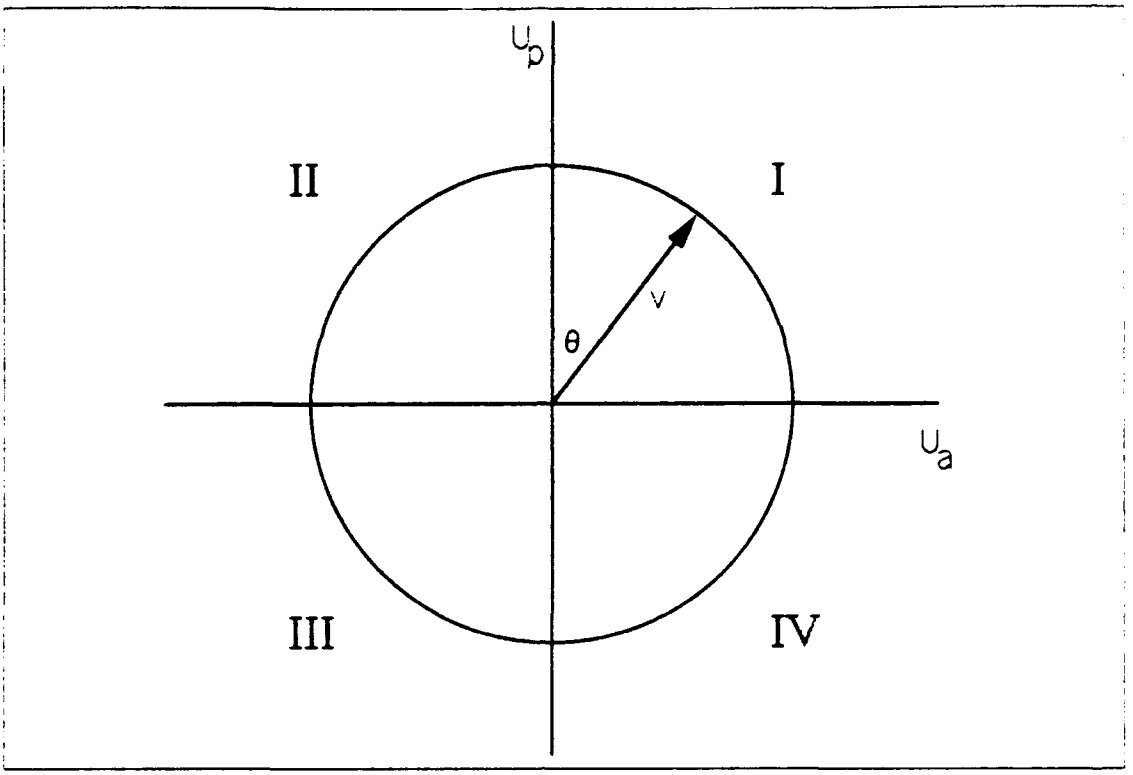

Figure 2.4 Four Quadrant Relationship of State Variables

Figure 2.6 is the proposed mapping of the lift and drag coefficients for the AUV II propeller as a function of effective angle of attack. This is an adaptation of the lift/drag coefficient model presented in reference 7 for cycloidal propellers. The curves in figure 2.6 assume no blade stall, which allows a continuous one term sinusoidal function to represent the mapping. This simple lift/drag model requires the identification of only one unknown parameter to characterize each coefficient curve, while retaining the physical amplitude and phase shift relationships for the lift and drag coefficients common to all airfoils. The equations for these curves are;

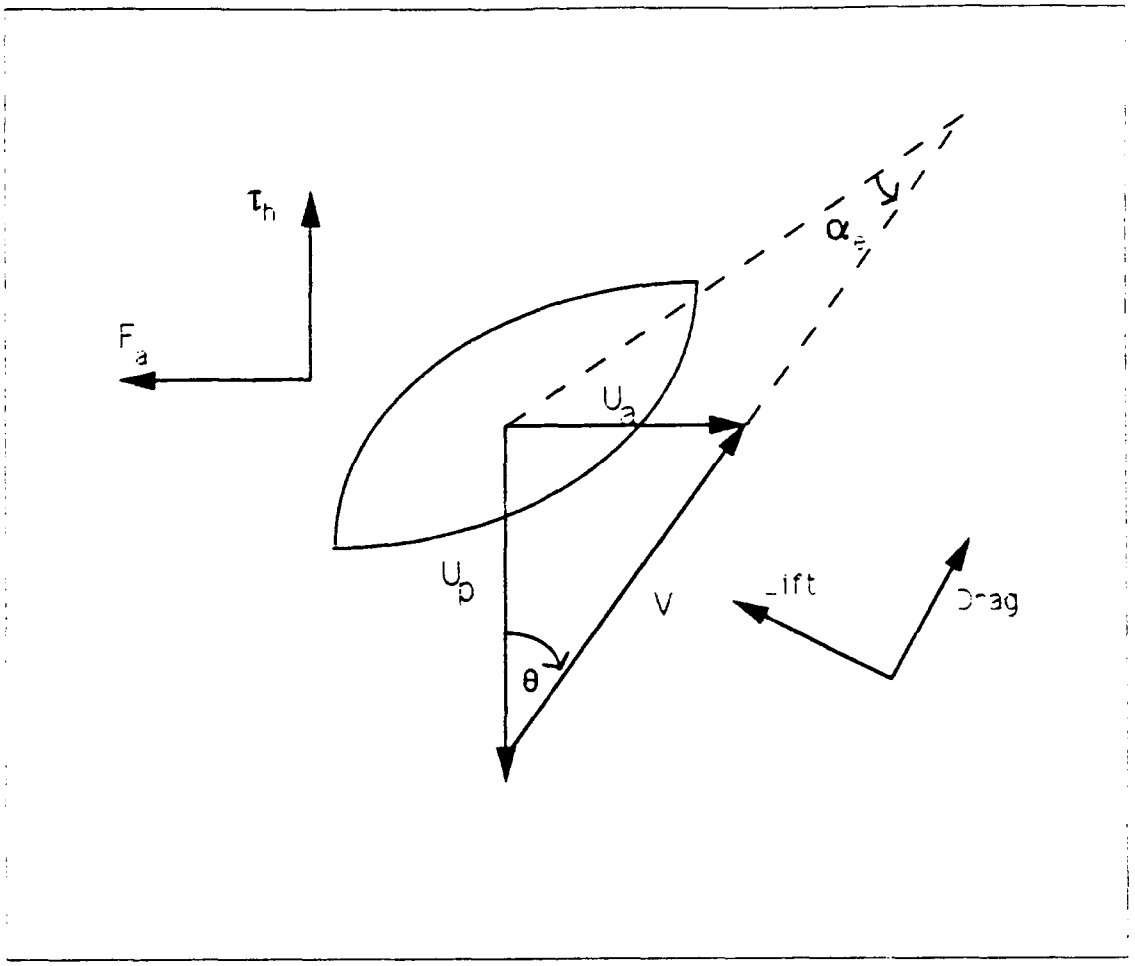

Figure 2.5 Simple Airfoil Theory Applied To A Propeller Blade

$$C_L = C_{L\max} \sin(2\alpha_e)$$

$$C_D = C_{D\max}(1 - \cos(2\alpha_e)) \tag{2.8}$$

Even though the assumption of no blade stall and zero drag at zero effective angle of attack deviates from known airfoil theory, the simplicity these assumptions afford the model development outweighs the small inaccuracy introduced by the assumptions.

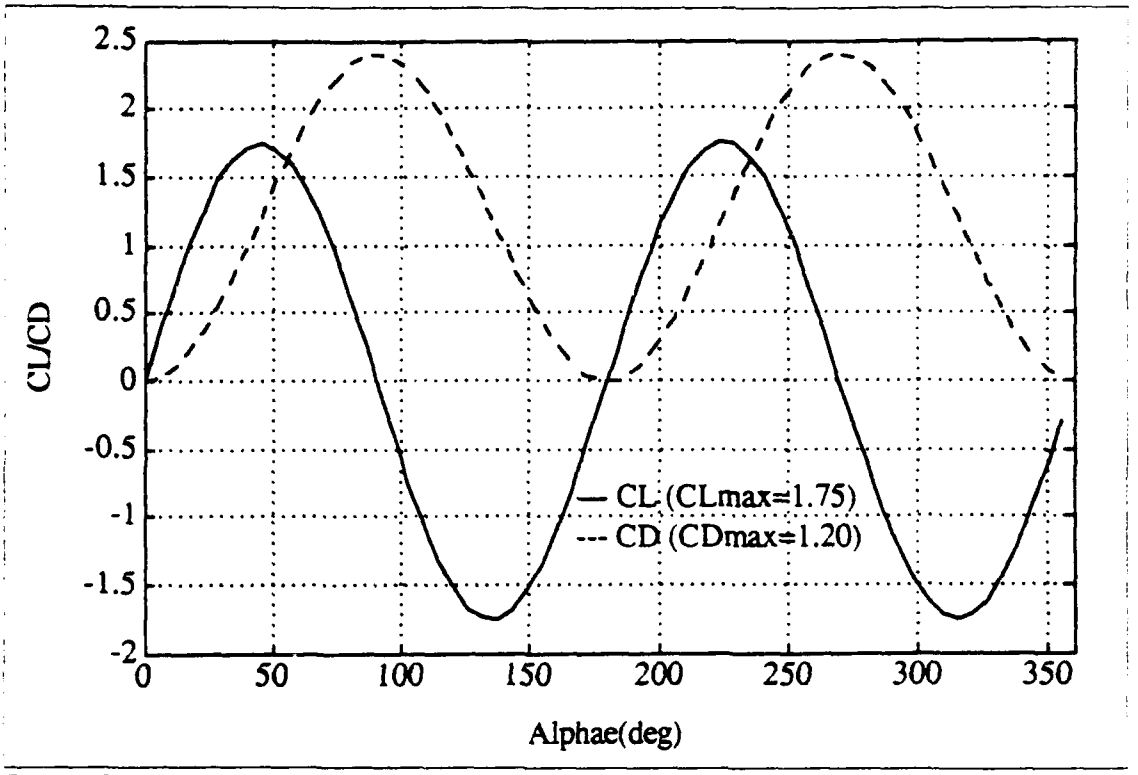

Figure 2.6 Lift and Drag Coefficients

Once known, the lift/drag coefficients and the total velocity vector can be translated into actual lift and drag forces by the following equations.

$$\text{Lift} = \left(\frac{1}{2}\rho v^2 A\right) C_L$$

$$\text{Drag} = \left(\frac{1}{2}\rho v^2 A\right) C_D$$

The lift and drag forces are resolved into axial thrust and transverse force.

$$F_a = \text{Lift}(\cos(\theta)) - \text{Drag}(\sin(\theta))$$

$$F_t = \text{Lift}(\sin(\theta)) + \text{Drag}(\cos(\theta))$$

Finally, the transverse force is converted to hydrodynamic torque.

$$\tau_{hydro} = 0.7\left(\frac{D}{2}\right)F_t$$

Using this approach, the axial force and hydrodynamic torque are functions of the system state variables, and the system dynamic equations 2.7 become;

$$\begin{aligned} \dot{\omega}_M &= g_1(\omega_M, U_a, V_a) \\ \dot{U}_a &= g_2(\omega_M, U_a) \end{aligned} \tag{2.9}$$

The system is modeled by two coupled nonlinear first order differential equations that are a function of the state variables and the voltage input. Simulation of AUV II thruster performance can readily be performed with the system dynamic equations in this form.

III. DYNAMIC MODEL VALIDATION

A. THRUSTER TANK TESTS

The experimental data used to validate the model derived in Chapter II was obtained by Cody [Ref. 1]. Figure 3.1 is a diagram of the test setup use at the NPS test tank facility. An actual thruster assembly removed from the AUV II was used for the experiment with the exception that the servomotor was waterproofed so it could be immersed in the tank. Reference 1 describes the test equipment configuration and the calibration performed on the equipment.

The test program consisted of operating the thruster servomotor through an extensive range of control voltage inputs for several tunnel configurations. Triangular and square shaped input voltages were used with periods of 0.5 to 50 seconds with amplitudes ranging from 9.0 to 20.4 volts. Propellers with 45 and 30 degree pitch, and tunnel lengths of 10 and 16.5 inches were tested. Measurements were obtained for thruster axial force, motor angular velocity, applied voltage, and motor current. From this entire experiment, three specific sets of data were chosen for model validation. A tunnel configuration 16.5 inches long with a 45 degree pitch propeller was subjected to 20.4 maximum voltage inputs, with 2 second square wave, 2 and 50 second triangular wave signals.

The velocity of the water column in the tunnel was not measured. Therefore, the calculated values for the U_a state were not compared to actual data, only predicted axial

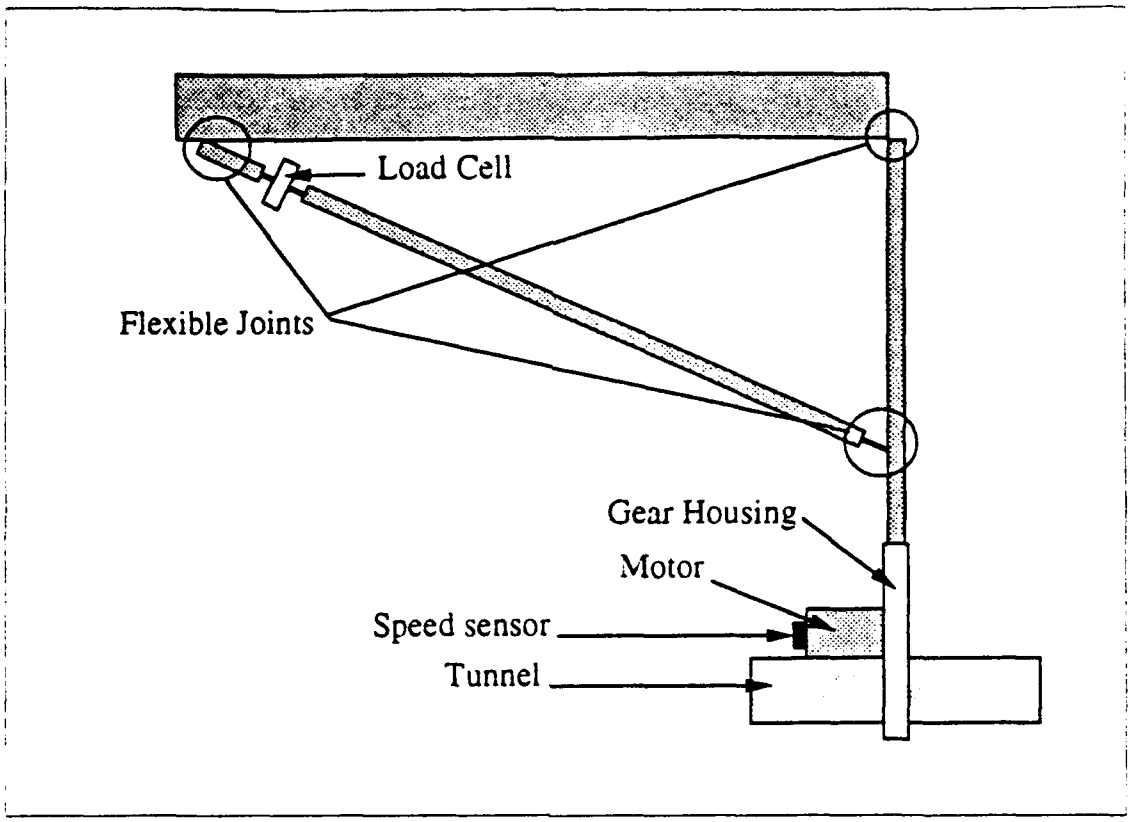

Figure 3.1 Test Frame Assembly

force and motor speed were compared to experimental data for validation.

B. PARAMETER IDENTIFICATIONS

The physical constants use to derive the thruster dynamic equations 2.7 that have known values determined by system and component design are listed in Appendix A. Four parameters associated with the specific design of this tunnel and the propeller blades were determined empirically by matching the model output with the experimental data. These parameters are the inertial factor γ, and the momentum correlation factor $\Delta\beta$ in equation 2.5; the maximum lift and drag coefficients C_{Lmax} and C_{Dmax} in equation 2.8. No

attempt was made to derive the actual values for these parameters, even though a range for their expected values are known from experience with similar systems.

C. VALIDATION

The model was matched to one particular set of experimental data, then compared to two other sets of data for evaluation. The set of data used for determining the four parameter mentioned above was the 2 second period, square wave with maximum motor voltage 20.4 volts. The entire set of system differential equations are coupled so no one parameter determined a particular attribute, but in general changing γ and C_{Lmax} matched the force transient peak, $\Delta\beta$ and C_{Lmax} fixed the steady state force output, and C_{Dmax} was varied to match calculated and actual motor velocity. The four parameters are restricted to a range of approximately 1.0 +/- 1.0, to maintain physical reality for the system's model. The model output and experimental data were qualitatively matched while keeping the parameters in a range that made physical sense. Figure 3.2 is the model output compared to the experimental data with the following parameter selection:

- $C_{Lmax} = 1.75$
- $C_{Dmax} = 1.20$
- $\gamma = 0.5$
- $\Delta\beta = 0.2$

The values for these parameters are comparable to other airfoil or control volume system models.

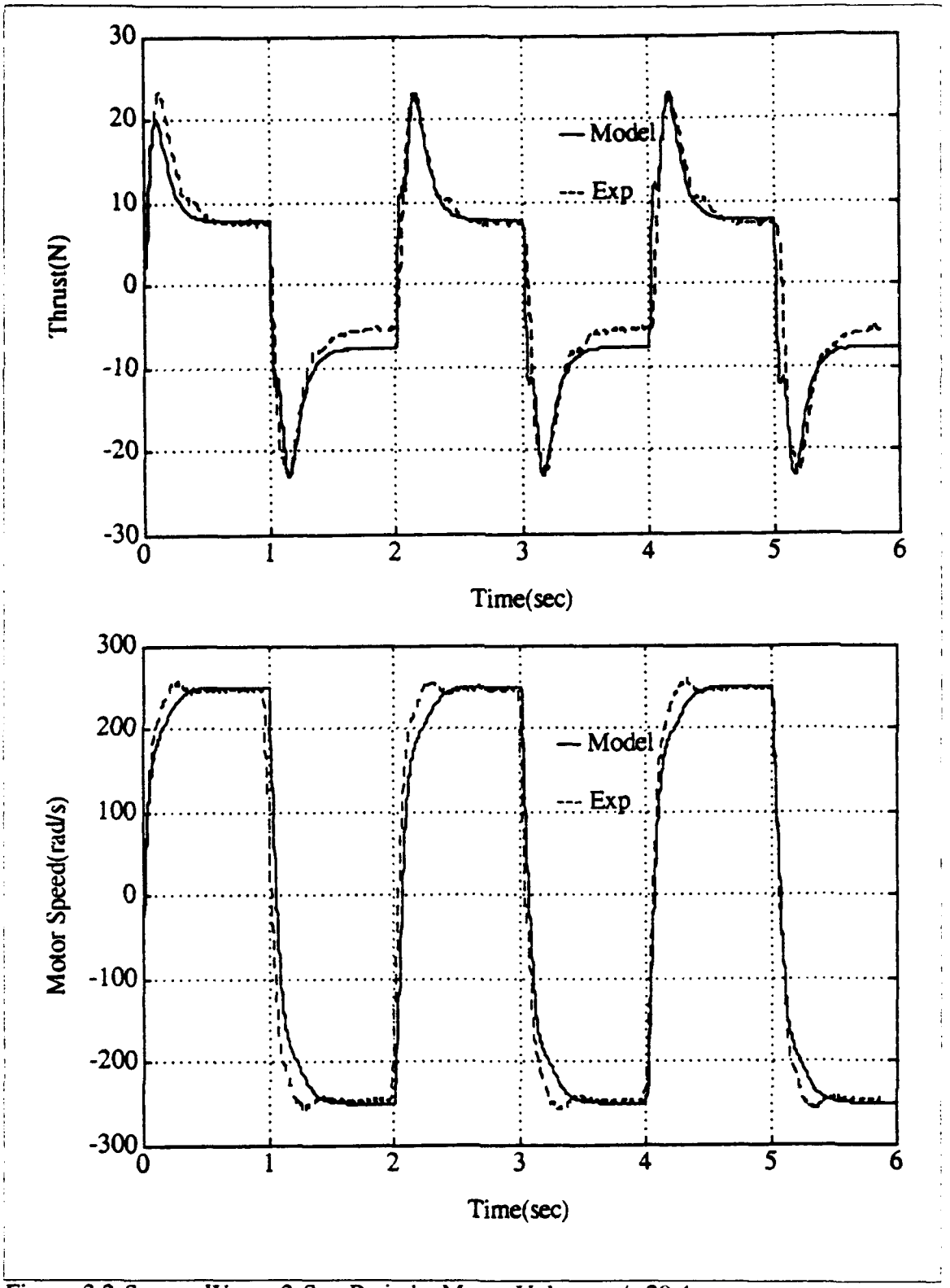

Figure 3.2 Square Wave, 2 Sec Period, Motor Voltage +/- 20.4 v

Non-linear dynamic systems like this model can not be analyzed for frequency response and step response as is done for linear systems. The two second square wave input period was selected as the test case for tuning this model because it subjected the model to both transient and steady state conditions similar to a step input analysis of a linear system. The model was able to meet the criteria state above and matched the data closely. The model was then simulated with triangular voltage inputs of two and fifty second periods, 20.4 volts maximum motor voltage. The output was compared to the two corresponding sets of data. Figures 3.2 and 3.3 present the results of this simulation. Triangular wave voltage inputs are analogous to sine wave inputs use for frequency response testing of linear systems where high and low frequency response of the system's model can be observed. The long fifty second period input can be considered essentially steady state response.

D. EVALUATION

The propeller was designed to have symmetrical operating characteristics in both the forward and reverse directions. The experimental data indicates however, that the thrust produced by the propeller is slightly higher in the forward direction. The model output is symmetric for positive and negative voltage input which presents a problem how to best identify the parameters and match the data. It was decided to match only the forward steady state thrust and not to incorporate this asymmetry into the model. Also the experimental data exhibits a slight overshoot for motor angular velocity. The model output has no motor speed overshoot. While the reasons for this are not totally defined,

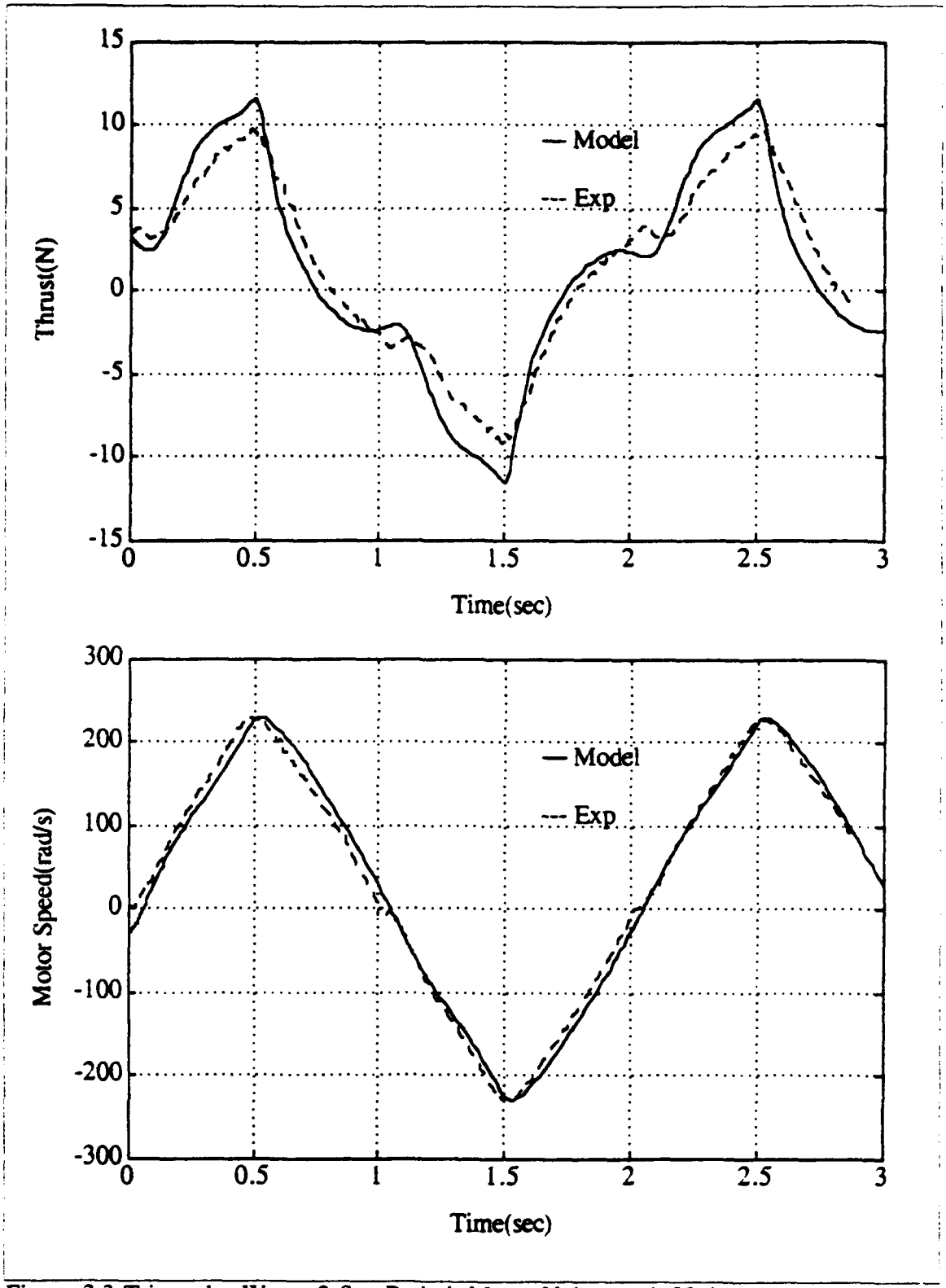

Figure 3.3 Triangular Wave, 2 Sec Period, Motor Voltage +/- 20.4 v

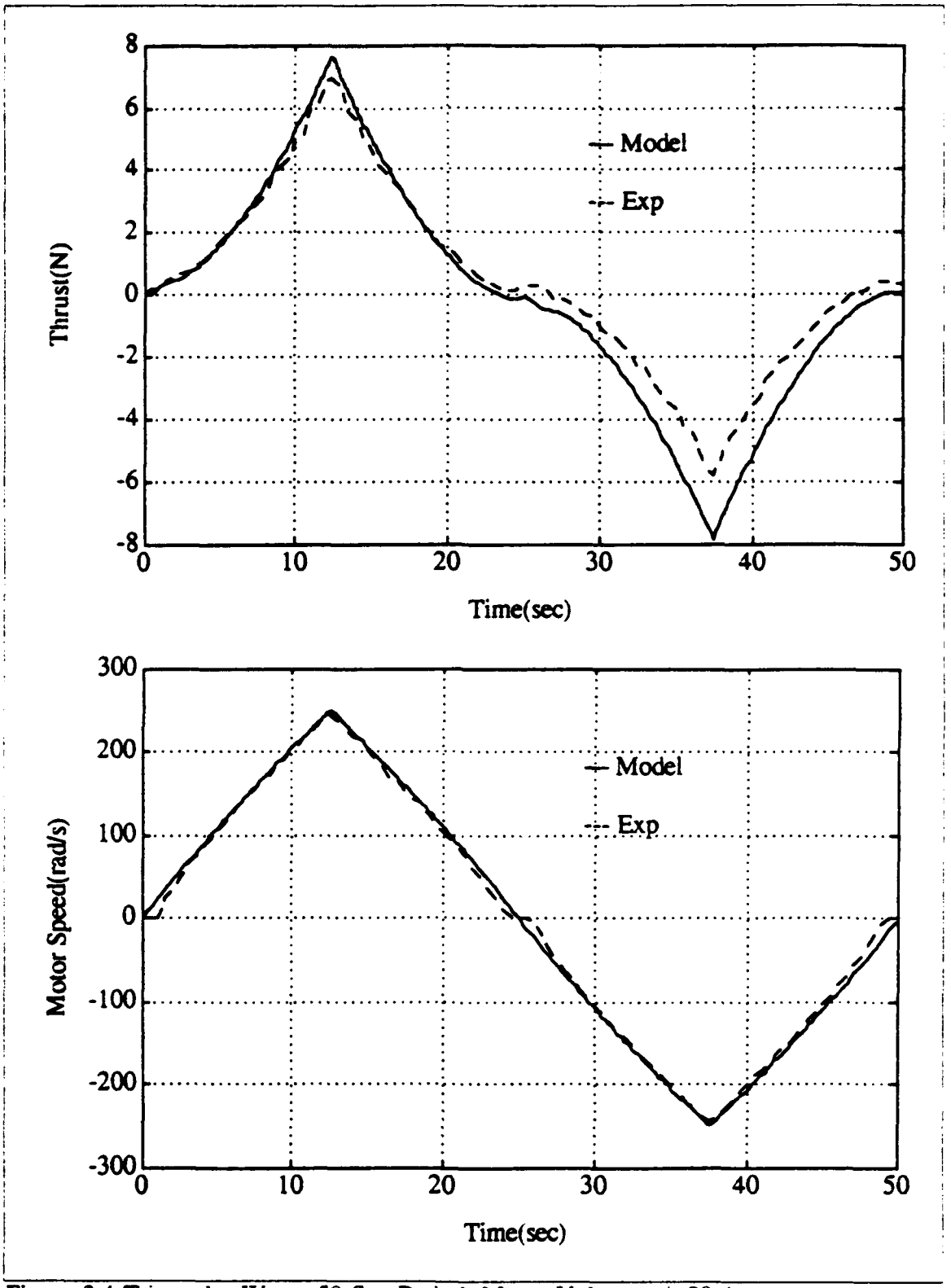

Figure 3.4 Triangular Wave, 50 Sec Period, Motor Voltage +/- 20.4 v

it is possible that neglecting motor inductive effects could account for the over damping of the model. It follows that only steady state motor speed was possible to match. But for the these two exceptions, the model replicated the experimental data exactly using the values for the parameters identified above. The four parameters where held constant for the subsequent simulations of the other signal responses.

Figure 3.3 shows the model's dynamic response to a two second cyclic input. While the motor speed predicted by the model matched the data closely, predicted thrust was high as the motor speed increased and slightly low during the down ramp. The acceleration of the water column will influence the thrust output throughout this entire cycle. Therefore the inertial term is distorting the model output. This could be attributed to the γ inertial factor, which is a function of the velocity profile of the water column, being slightly different during triangular voltage inputs. Additionally the lift and drag coefficients are not pure sine functions, and the errors introduced by this assumption are more significant during transient flows. The similarity of the wave shapes does indicate that during transient conditions, where changing angles of attack dominates the dynamic behavior of the system, the four quadrant concept replicates this phenomena closely.

A significant feature of the dynamic response is that the peak thrust coincides exactly in time with that observed in the experimental data. The four quadrant model resolves the lead/lag dilemma between the NPS and WHOI models discussed in Chapter II.

Figure 3.4 demonstrates the static response to a long fifty second cyclic input. With the exception of the forward/reverse asymmetry for thrust, predicted output matched

experimental data in both shape of the curves and magnitude. Since during this cycle when the momentum term dominates, the model's steady state prediction is very accurate.

The comparison between the simulation and experimental data was deemed successful and no modification was made to the model. The system differential equations 2.9 together with the identified parameters were use for the development of the control scheme as explained in the next chapter.

IV. AUV II THRUSTER CONTROL

A. INVERSE STATIC MAP

Hovering is accomplished by the AUV II when the navigation force allocation subsystem commands the thrusters to produce a desired force to move the vehicle to a position required for the mission. Proper control of the thruster should produce an identical axial force output as the command force input over a desired frequency range. This chapter will describe a control scheme for the thruster that compensates for the nonlinear relationship between the thruster's motor voltage input and axial force output to give the desire linear relationship. This will be for low frequency operations, when the system's static characteristics dominates the output behavior. The control law at the first level of precision will be an inverse static map as described by the block diagram in Figure 4.1. A force command input F_c to the thruster will produce a linear force output F_a.

Inspection of equations 2.4 and 2.5 reveals that in steady state conditions when the acceleration terms go to zero, a square law relationship exists between the thruster voltage input and force output. Figure 4.2 is a plot of the model's predicted axial force output for a fifty second triangular wave voltage input. Except for some hysteresis at the origin, this is a square law relationship with sign preserved for forward and reverse directions. A least square fit between F_a and v^2 calculates the linear slope for the plant's square law static map.

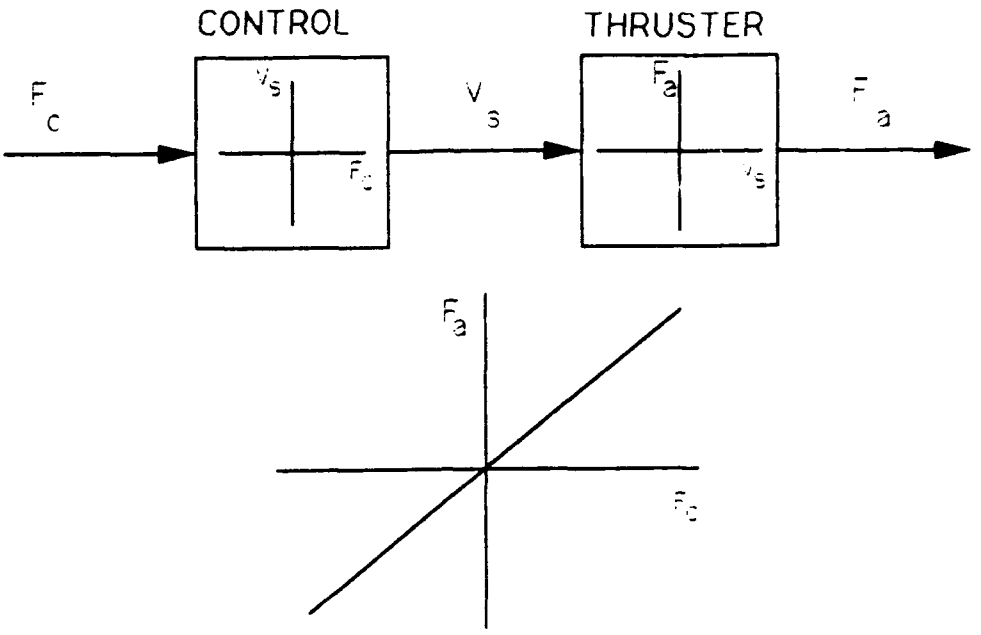

Figure 4.1 Open Loop Inverse Static Map Control

$$F_a = \delta(V_s|V_s|) \tag{4.1}$$

The inverse of equation 4.1 is the control law interface between the force allocation logic and the thruster.

$$V_s = \sqrt{\frac{F_c}{\delta}}(\text{sign}F_c) \tag{4.2}$$

This open loop inverse static map control was simulated for high and low frequency command force inputs to determine expected thruster force outputs.

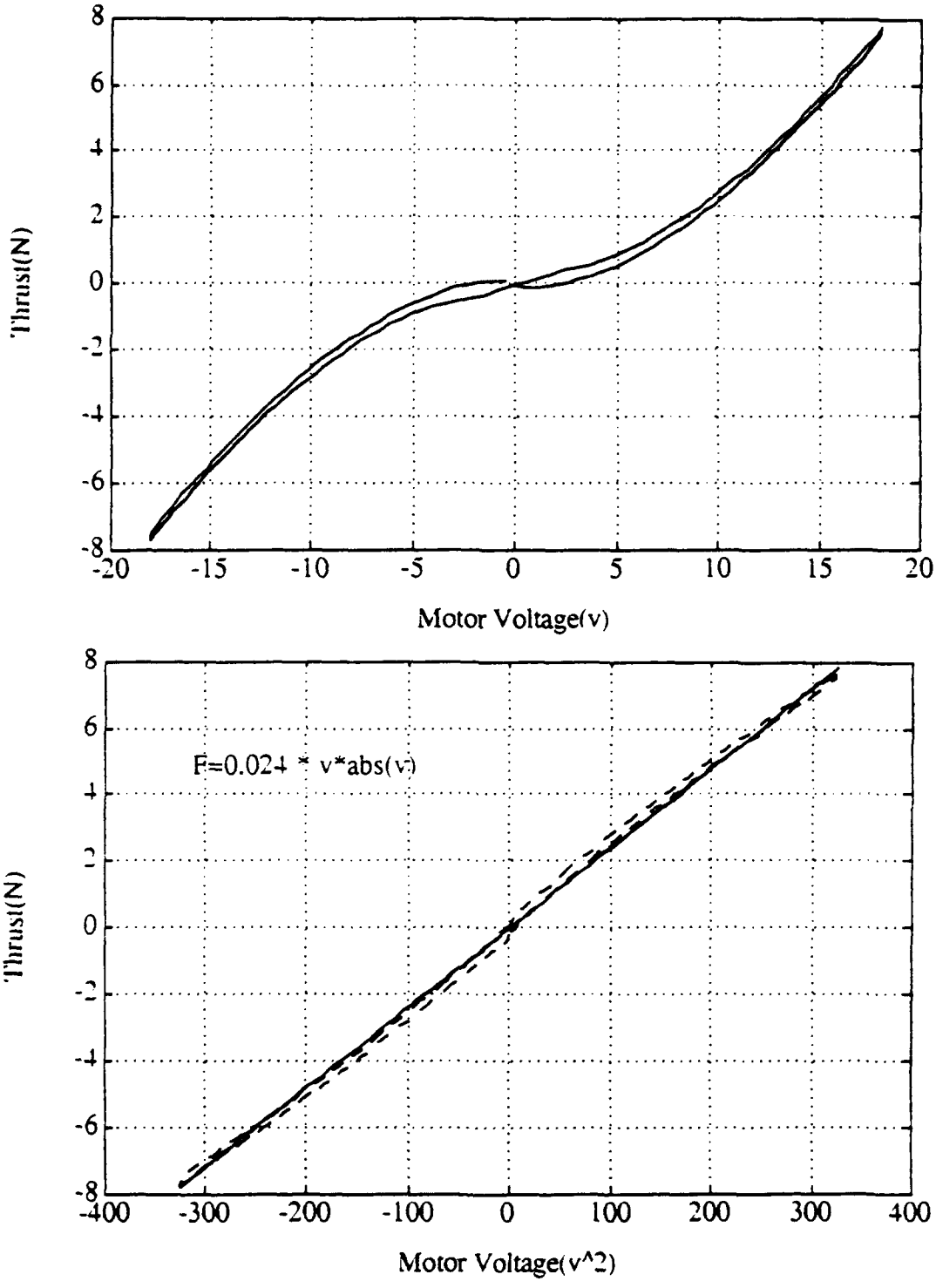

Figure 4.2 Force/Voltage Static Map

B. PERFORMANCE OF INVERSE STATIC MAP CONTROLLER

The thruster output was simulated for two command force F_c inputs using the control law developed above. The fifty second period triangular wave command force input demonstrates the system's low frequency response while the five second period input reveals system dynamic response. Figure 4.3 only deviates from command briefly when the motor changes directions. Inspection of the state variables' behavior during the simulation indicated that transient peaks in thrust during flow reversals is due to a step change in motor speed causing a spike in the effective angle of attack.

C. SYSTEM STATE VARIABLES

Figure 4.4 is a plot of both system state variables U_a and U_p during the low frequency command input. Qualitatively this relationship makes physical sense with water column velocity lagging slightly behind propeller velocity while the propeller is changing speeds. As illustrated in Figure 2.4, the relationship between U_a and U_p determines the effective angle of attack of the water column on the blades, which in turn determines the propeller's lift and drag coefficients. Figure 4.5 shows the effective angle of attack during the complete cycle. Except for when the propeller changes direction, effective angle of attack is approximately four degrees. The spike in effective angle of attack during flow reversals is probably an anomaly and is what causes the transients peaks in thrust output during simulation. Even though the propeller can change direction very rapidly, the actual change in the angle of attack of the water column on the blades is probably a smooth continuous transition.

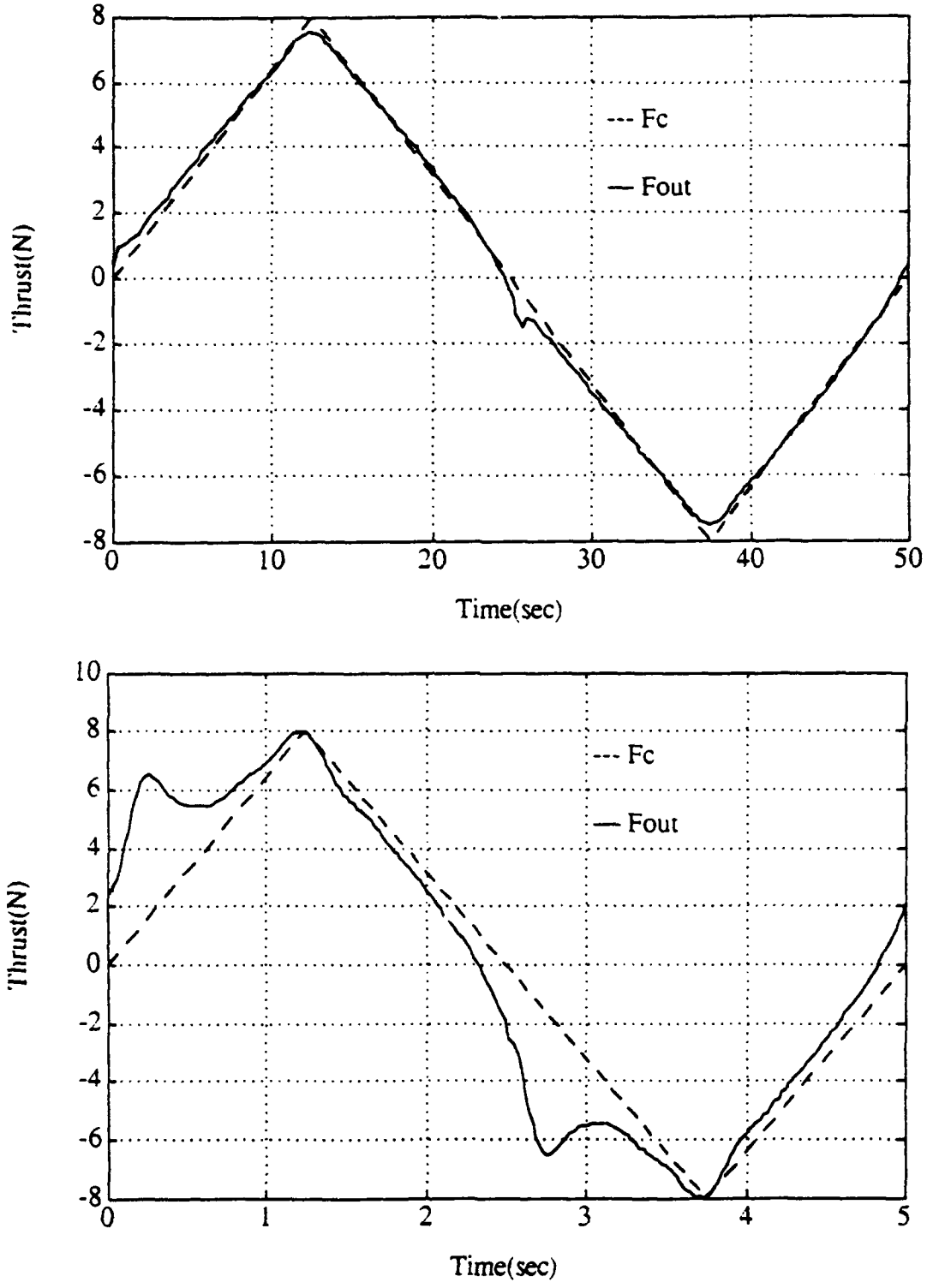

Figure 4.3 Controller Simulation For Command Force Input

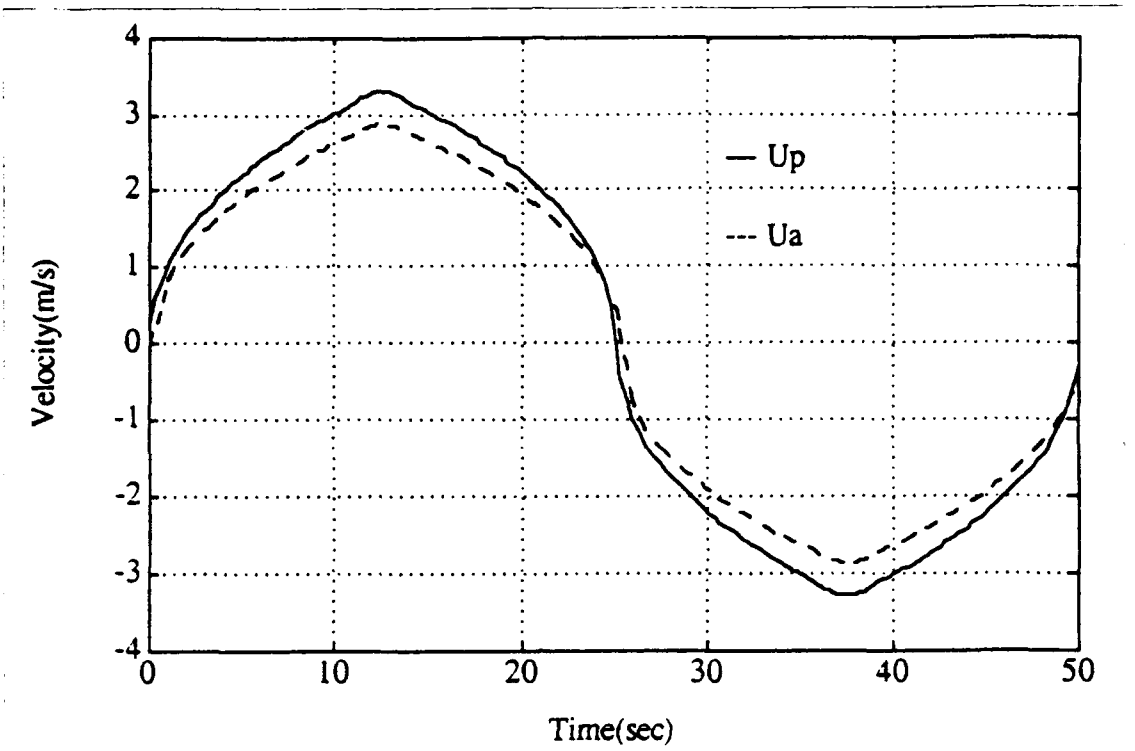

Figure 4.4 System State Variables Low Frequency Response

Further refinements to both the theoretical model and the control law will occur after actual field testing of the control law in the AUV II.

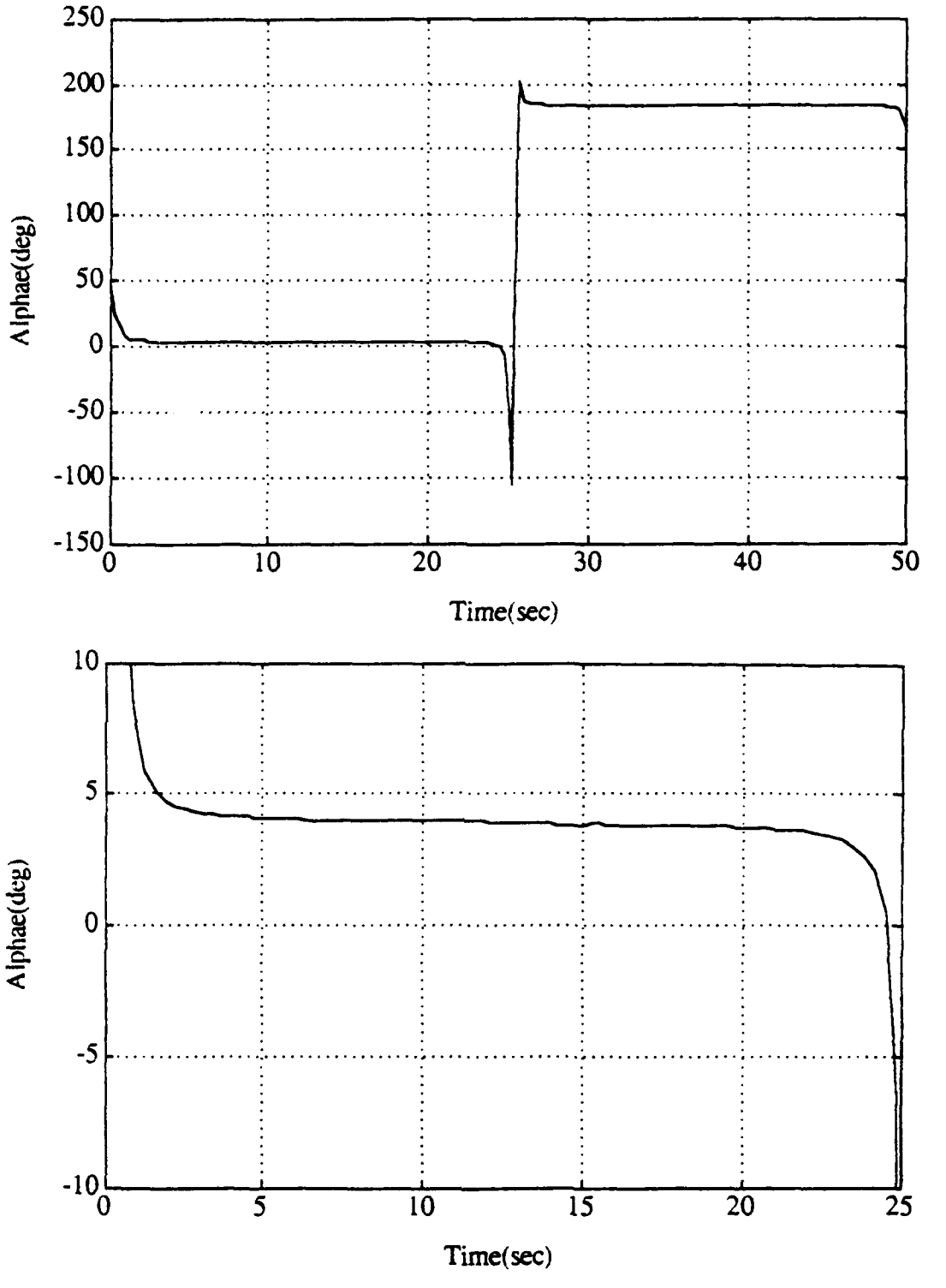

Figure 4.5 Effective Angle Of Attack

V. CONCLUSIONS

A. CONCLUSIONS

The rapid response of small tunnel thrusters necessitates an understanding of the full dynamic range of thruster operation. This is accomplished by incorporating a four quadrant map of the propeller's force and torque characteristics into the system dynamic model while keeping the number of disposable parameters to a minimum.

It was shown that the four quadrant mapping of propeller blade lift/drag coefficients as a function of effective angle of attack proposed in Chapter II predicted very accurate results for the AUV II thrusters force output when compared to actual experimental data, utilizing a simplified but physically reasonable representations of the propeller's lift and drag characteristics. The use of only four empirical hydrodynamic parameters allowed two degrees of freedom to model propeller blade lift and drag performance, and two degrees of freedom to model the tunnel/water column mass and momentum characteristics. With the propellers thrust output as a function of angle of attack on the blades, the transient peak of square wave response matched the experimental data very closely.

The inverse static map control law produces good linear correlations between low frequency command force input signals and thruster output for the expected bandwidth of the AUV's operations. If in water testing of the AUV II indicates dynamic

compensation is necessary, this improved dynamic model will facilitate the development of full sliding mode control for vehicle thruster control.

APPENDIX A

TABLE OF COEFFICIENTS

Coefficients	Symbol	Value
Area	A	0.00445 m^2
Diameter	D	0.0762 m
Length	L	0.4191 m
Motor Polar Moment of Inertia	J_M	1.63e-5 kg m^2
Pinion Polar Moment of Inertia	J_{IXi}	0.3186e-5 kg m^2
Propeller Polar Moment of Inertia	J_P	3.4481e-5 kg m^2
Motor Shaft Friction	C_M	0.00022
Propeller Shaft Friction	C_P	0.0
Motor Electrical Resistance	R	1.73 ohms
Motor Back EMF Constant	K_M	0.055 volt/rad/sec
Motor Torque Constant	K_T	0.0551 N m/amp
Reduction Gear Ratio	N	2
Water Density	ρ	998.0 kg/m^3

APPENDIX B

```
% FOUR QUADRANT DYNAMIC AUV II THRUSTER MODEL
% This is the driver program for the system dynamic model
% It defines system parameters and integrates the Differential Equations
% 27 APRIL 1993   LCDR JAMES P. BROWN

global T N A D Vmax K0 K1 K2 K3 K4 Rho pitch
clear;clg

% Known Parameters/Constants
T = 5.0;                    % simulation duration
Vs =8;                      % peak control voltage signal (v)
Vmax =  Vs*2.272;           % peak voltage to motor
D = 0.0762;                 % tube diameter (m)
L = .4191;                  % tube length (m)
A = 4.5604e-3;              % cross sectional area (m^2)
Jm = 1.63e-5;               % motor inertia (kg*m^2)
Jdg = 0.3186e-5;            % drive gear inertia (kg*m^2)
Jp = 3.4481e-5;             % propeller inertia (kg*m^2)
Cm = 0.00022;               % motor viscous friction
Cp = 0.0;                   % propeller shaft viscous friction
R = 1.73;                   % motor resistance (ohms)
Km = 0.055;                 % motor constant (volts/(rad/sec))
Kt = 0.0551;                % motor torque constant (N*m/A)
gamma=0.5;                  % inertial factor
N = 2.0;                    % reduction gear ratio
pitch=pi/4;                 % prop 45 deg pitch
delB = 0.2;                 % delta beta
Rho = 998.0;                % density H20 (kg/m^3)

% System Equation Coefficients
K0 = Cm + Cp/N^2 + Kt*Km/R;
K1 = Kt/R;
K2 = Jm + Jdg + Jp/N^2;
K3 = Rho*A*L*gamma;
K4 = Rho*A*delB;

t0=0.0; tf=T; x0=[0;0];
[t,x]=ode45('dynamics',t0,tf,x0,0.001);

% Use the state variables to reconstitute system variables
[l]=length(t);temp=zeros(5,1);
for i=1:l, [xdot,output]=dynamics(t(i),x(i,:));temp(:,i)=output;end;
alphae=temp(1,:);Ua=temp(2,:);Up=temp(3,:);F=temp(4,:);v=temp(5,:);

plot(t,F),grid
```

APPENDIX C

```
% FOUR QUADRANT DYNAMIC PROPELLER MODEL
% This program formulates the nonlinear coupled
% differential equations for thruster dynamics
% 27 APRIL 93   LCDR JAMES P. BROWN

function [xdot,output] = dynamics(t,x)

% Triangular Fourier Series
Tp=5;Fmax=8; %cycle period and amplitude
s3=[1 3 5 7 9 11 13 15]';s4=[1 -3 5 -7 9 -11 13 -15]';
s2=sin(s3*(2*pi/Tp)*t)./s3 ./s4 ;s1=(8/pi^2)*sum(s2);
Fc= Fmax * s1;

% Inverse Static Map Control Law
v=sqrt(41.018*abs(Fc))*sign(Fin); %motor voltage input


Ua=x(1); wm=x(2); wp=x(2)/N;
Up=0.7*wp*D/2;
V2=(Ua^2+Up^2);

theta=atan2(Ua,Up);      %relative flow angle
alphae=(pi/2-pitch)-theta;%angle of attack

CL=1.75*sin(2*alphae);  %lift coef
CD=1.2*(1-cos(2*alphae));%drag coef

Lift=(0.5*Rho*V2) * A * CL;
Drag=(0.5*Rho*V2) * A * CD;

Fa=Lift*cos(theta) - Drag*sin(theta);%axial force
Ft=Lift*sin(theta) + Drag*cos(theta);%trans force
tau=0.7 * D/2 * Ft;      %hydraulic torque

% System Differential Equations
Uadot=(Fa - K4*Ua*abs(Ua))/K3;
wmdot=-(K0/K2)*wm + (K1/K2)*v - tau/(N*K2);

xdot=[Uadot;wmdot];
output=[alphae;Ua;Up;Fa;v];
```

LIST OF REFERENCES

1. Cody, S.E., An Experimental Study of the Response of Small Thrusters to Triangular and Square Wave Inputs, Master's Thesis, Naval Postgraduate School, Monterey, California, December 1992.

2. McLean, M.B., Dynamic Performance of Small Diameter Tunnel Thrusters, Master's Thesis, Naval Postgraduate School, Monterey, California, March 1991.

3. Yoerger, D.R., Cooke, J.G., and Slotine, J.-J.E., "The Influence of Thruster Dynamics on Underwater Vehicle Behavior and Their Incorporation into Control System Design," IEEE Journal of Ocean Engineering, Volume 15, Number 3, pp. 167-177, July 1990.

4. Miles, D., Burton, D., Lee, M., and Rock, S., Closed Loop Force Control of an Underwater Thruster, Monterey Bay Aquarium Research Institute/Stanford Aeronautics Robotics Laboratory, Monterey/Palo Alto, California, October 1992.

5. Adams, J.C., Burton, D., and Lee, M., Dynamic Characterization and Control of Thrusters for Underwater Vehicles, Monterey Bay Aquarium Research Institute/Stanford Aeronautics Robotics Laboratory, Monterey/Palo Alto, California, September 1991.

6. van Lammeren, W.P.A., van Manen, J.D., Oosterveld, M.W.C., "The Wageningen B-Screw Series," The Society of Naval Architects and Marine Engineers, Volume 77, pp. 269-317, November 1969.

7. Rickards, M.A., "Cycloidal Propulsion of Submersibles, "Journal of Hydronautics, Volume 4, Number 2, pp. 66-72, April 1970.

INITIAL DISTRIBUTION LIST

		No. Copies
1.	Defense Technical Information Center Cameron Station Alexandria VA 22304-6145	2
2.	Library, Code 052 Naval Postgraduate School Monterey CA 93943-5002	2
3.	Chairman, Code ME/KK Department of Mechanical Engineering Naval Postgraduate School Monterey CA 93943-5000	1
4.	Naval Engineering Curricular Office, Code 34 Naval Postgraduate School Monterey CA 93943-5000	1
5.	Dr. Anthony J. Healey, Code ME/HY Department of Mechanical Engineering Naval Postgraduate School Monterey CA 93943-5000	2
6.	Dr. Dana Yoerger Woods Hole Oceanographic Institute Woods Hole MA 02543-5000	1
7.	Chris Agoras/Chris Hellenbaum Naval Underwater Systems Center (NUSC) Newport RI 02841-5047	1
8.	Mike Lee 160 Central Ave Pacific Grove CA 93950-5000	1

9. Dr. Stephen Rock 1
Department of Aeronautics and Astronautics
Stanford University
Stanford CA 94305-5000

10. LCDR James P. Brown 1
Portsmouth Naval Shipyard
Portsmouth NH 03804-5000